

# International Journal of Physical Sciences

Volume 12 Number 20 30 October , 2017

ISSN 1992-1950



*Academic  
Journals*

## ABOUT IJPS

The **International Journal of Physical Sciences (IJPS)** is published weekly (one volume per year) by Academic Journals.

**International Journal of Physical Sciences (IJPS)** is an open access journal that publishes high-quality solicited and unsolicited articles, in English, in all Physics and chemistry including artificial intelligence, neural processing, nuclear and particle physics, geophysics, physics in medicine and biology, plasma physics, semiconductor science and technology, wireless and optical communications, materials science, energy and fuels, environmental science and technology, combinatorial chemistry, natural products, molecular therapeutics, geochemistry, cement and concrete research, metallurgy, crystallography and computer-aided materials design. All articles published in IJPS are peer-reviewed.

### Contact Us

**Editorial Office:** [ijps@academicjournals.org](mailto:ijps@academicjournals.org)

**Help Desk:** [helpdesk@academicjournals.org](mailto:helpdesk@academicjournals.org)

**Website:** <http://www.academicjournals.org/journal/IJPS>

**Submit manuscript online** <http://ms.academicjournals.me/>

## Editors

### **Prof. Sanjay Misra**

*Department of Computer Engineering, School of Information and Communication Technology  
Federal University of Technology, Minna,  
Nigeria.*

### **Prof. Songjun Li**

*School of Materials Science and Engineering,  
Jiangsu University,  
Zhenjiang,  
China*

### **Dr. G. Suresh Kumar**

*Senior Scientist and Head Biophysical Chemistry  
Division Indian Institute of Chemical Biology  
(IICB)(CSIR, Govt. of India),  
Kolkata 700 032,  
INDIA.*

### **Dr. Remi Adewumi Oluyinka**

*Senior Lecturer,  
School of Computer Science  
Westville Campus  
University of KwaZulu-Natal  
Private Bag X54001  
Durban 4000  
South Africa.*

### **Prof. Hyo Choi**

*Graduate School  
Gangneung-Wonju National University  
Gangneung,  
Gangwondo 210-702, Korea*

### **Prof. Kui Yu Zhang**

*Laboratoire de Microscopies et d'Etude de  
Nanostructures (LMEN)  
Département de Physique, Université de Reims,  
B.P. 1039. 51687,  
Reims cedex,  
France.*

### **Prof. R. Vittal**

*Research Professor,  
Department of Chemistry and Molecular  
Engineering  
Korea University, Seoul 136-701,  
Korea.*

### **Prof Mohamed Bououdina**

*Director of the Nanotechnology Centre  
University of Bahrain  
PO Box 32038,  
Kingdom of Bahrain*

### **Prof. Geoffrey Mitchell**

*School of Mathematics,  
Meteorology and Physics  
Centre for Advanced Microscopy  
University of Reading Whiteknights,  
Reading RG6 6AF  
United Kingdom.*

### **Prof. Xiao-Li Yang**

*School of Civil Engineering,  
Central South University,  
Hunan 410075,  
China*

### **Dr. Sushil Kumar**

*Geophysics Group,  
Wadia Institute of Himalayan Geology,  
P.B. No. 74 Dehra Dun - 248001(UC)  
India.*

### **Prof. Suleyman KORKUT**

*Duzce University  
Faculty of Forestry  
Department of Forest Industrial Engineering  
Beciyorukler Campus 81620  
Duzce-Turkey*

### **Prof. Nazmul Islam**

*Department of Basic Sciences &  
Humanities/Chemistry,  
Techno Global-Balurghat, Mangalpur, Near District  
Jail P.O: Beltalpark, P.S: Balurghat, Dist.: South  
Dinajpur,  
Pin: 733103,India.*

### **Prof. Dr. Ismail Musirin**

*Centre for Electrical Power Engineering Studies  
(CEPES), Faculty of Electrical Engineering, Universiti  
Teknologi Mara,  
40450 Shah Alam,  
Selangor, Malaysia*

### **Prof. Mohamed A. Amr**

*Nuclear Physic Department, Atomic Energy Authority  
Cairo 13759,  
Egypt.*

### **Dr. Armin Shams**

*Artificial Intelligence Group,  
Computer Science Department,  
The University of Manchester.*

## Editorial Board

**Prof. Salah M. El-Sayed**

*Mathematics. Department of Scientific Computing,  
Faculty of Computers and Informatics,  
Benha University. Benha ,  
Egypt.*

**Dr. Rowdra Ghatak**

*Associate Professor  
Electronics and Communication Engineering Dept.,  
National Institute of Technology Durgapur  
Durgapur West Bengal*

**Prof. Fong-Gong Wu**

*College of Planning and Design, National Cheng Kung  
University  
Taiwan*

**Dr. Abha Mishra.**

*Senior Research Specialist & Affiliated Faculty.  
Thailand*

**Dr. Madad Khan**

*Head  
Department of Mathematics  
COMSATS University of Science and Technology  
Abbottabad, Pakistan*

**Prof. Yuan-Shyi Peter Chiu**

*Department of Industrial Engineering & Management  
Chaoyang University of Technology  
Taichung, Taiwan*

**Dr. M. R. Pahlavani,**

*Head, Department of Nuclear physics,  
Mazandaran University,  
Babolsar-Iran*

**Dr. Subir Das,**

*Department of Applied Mathematics,  
Institute of Technology, Banaras Hindu University,  
Varanasi*

**Dr. Anna Oleksy**

*Department of Chemistry  
University of Gothenburg  
Gothenburg,  
Sweden*

**Prof. Gin-Rong Liu,**

*Center for Space and Remote Sensing Research  
National Central University, Chung-Li,  
Taiwan 32001*

**Prof. Mohammed H. T. Qari**

*Department of Structural geology and remote sensing  
Faculty of Earth Sciences  
King Abdulaziz UniversityJeddah,  
Saudi Arabia*

**Dr. Jyhwen Wang,**

*Department of Engineering Technology and Industrial  
Distribution  
Department of Mechanical Engineering  
Texas A&M University  
College Station,*

**Prof. N. V. Sastry**

*Department of Chemistry  
Sardar Patel University  
Vallabh Vidyanagar  
Gujarat, India*

**Dr. Edilson Ferneda**

*Graduate Program on Knowledge Management and IT,  
Catholic University of Brasilia,  
Brazil*

**Dr. F. H. Chang**

*Department of Leisure, Recreation and Tourism  
Management,  
Tzu Hui Institute of Technology, Pingtung 926,  
Taiwan (R.O.C.)*

**Prof. Annapurna P.Patil,**

*Department of Computer Science and Engineering,  
M.S. Ramaiah Institute of Technology, Bangalore-54,  
India.*

**Dr. Ricardo Martinho**

*Department of Informatics Engineering, School of  
Technology and Management, Polytechnic Institute of  
Leiria, Rua General Norton de Matos, Apartado 4133, 2411-  
901 Leiria,  
Portugal.*

**Dr Driss Miloud**

*University of mascara / Algeria  
Laboratory of Sciences and Technology of Water  
Faculty of Sciences and the Technology  
Department of Science and Technology  
Algeria*

**Prof. Bidyut Saha,**

*Chemistry Department, Burdwan University, WB,  
India*

**ARTICLE**

<b>Models for calculating monthly average solar radiation from air temperature in Swaziland</b>	<b>247</b>
Mgidi D. Dlamini, Alakaparampil J. Varkey and Simiso K. Mkhonta	
<b>A study of semi-annual variation of residual geomagnetic field and its association with solar and geomagnetic activity</b>	<b>255</b>
Egba Ibeabuchi G., Kalu Florence D., Okwesili Agatha N. and Okpala Kingsley C.	
<b>Radioactivity in building materials in Saudi Arabia: An overview of experimental method and Monte Carlo N-Particle (MCNP) calculation</b>	<b>263</b>
H. Alshammari, Abdulrahman Alghamdi and Ahmed Algammidi	

*Full Length Research Paper*

# Models for calculating monthly average solar radiation from air temperature in Swaziland

Mgidi D. Dlamini, Alakaparampil J. Varkey and Simiso K. Mkhonta\*

Department of Physics, University of Swaziland, P/Bag 4, Kwaluseni. M201, Swaziland.

Received 24 August, 2017; Accepted 29 September, 2017

**Solar radiation is an important energy source for mankind. Accurate data of solar radiation levels for a particular location is vital for optimum operation of solar energy transducers such as photovoltaic cells and solar thermal collectors. In this work, it is shown a linear relationship exist between monthly average temperatures and solar radiation in Swaziland. The correlation has been utilized to develop two mathematical models for the estimation of solar radiation: one from the measured monthly average temperatures and the other from the square-root of the difference between measured maximum and minimum monthly average temperatures. Both models fit the data well and can be applied to estimate solar radiation in other parts of the region.**

**Key words:** Solar energy, solar radiation, climatic data, solar radiation estimation.

## INTRODUCTION

Accurate knowledge of solar radiation levels for a particular location is a prerequisite for the determination of the performance of various solar energy transducers such as photovoltaic cells and solar thermal collectors. Solar radiation data is also important in disciplines such as building designs and agricultural processes, for example evapo-transpiration of plants. However, weather stations will, at times do not have data on solar radiation because the instruments for radiation measurement, such as pyranometers and solarimeters, may not be available. As a result, mathematical models have been developed and calibrated to estimate solar radiation in different parts of the world such as in Brazil (Dos Santos et al., 2014), Iran (Saffaripour et al., 2013), India (Bajpai and Singh,

2009), Algeria/Spain (Chegaar et al., 1998), China (Li et al., 2014a, b), Bangladesh (Datta and Datta, 2013), Chile (Meza and Varas, 2000), USA (Allen, 1997) and Nigeria (Umoh et al., 2014). These models estimate solar radiation as a function of meteorological parameters such as temperature, atmospheric pressure, relative humidity, sunshine hours, wind speed, cloud cover, and rainfall.

Minimal empirical models require an input of only one meteorological parameter to estimate solar radiation and they include sunshine-hours based models (Angstrom, 1924; Chegaar et al., 1998; Yang et al., 2006), air-temperature based models (Hargreaves and Samani, 1982; Bristow and Campbell, 1984; Allen, 1997, Dos Santos et al., 2014) and cloud cover based models

\*Corresponding author. E-mail: smkhonta@uniswa.sz.

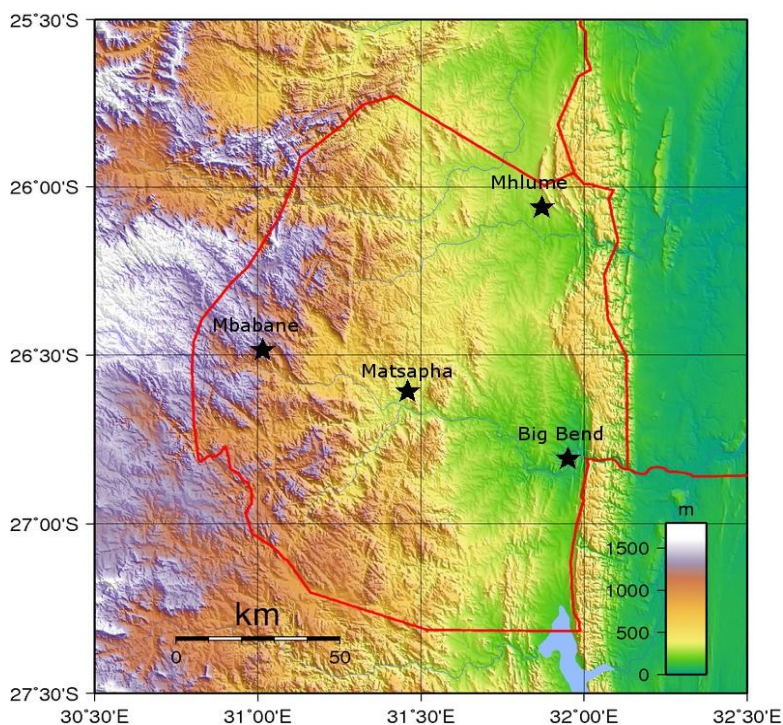


Figure 1. Topographic map of Swaziland.

Table 1. Areas of interest in the solar radiation estimation project.

Location	Climatic Region	Altitude (m)	Latitude (°S)	Longitude (°E)
Big Bend	Lowveld	150	26.82	31.93
Mhlume	Lowveld	258	26.00	31.90
Matsapha	Middleveld	640	26.50	31.32
Mbabane	Highveld	1150	26.30	31.13

(Kostic and Mikulovic, 2017). There are also intermediate models that require the input of two or more meteorological parameters (Okundamiya et al., 2016).

In Swaziland, a number of meteorological stations do not measure solar radiation, and the frequently available meteorological records are the daily maximum and minimum temperatures and precipitation. For this reason, this paper evaluates two air-temperature based models for predicting monthly solar radiation in four locations within Swaziland. At one location, measured solar radiation values are available to correctly adjust the empirical coefficients of the models and also to compare with results from other parts of the world.

### CLIMATIC CONDITIONS IN SWAZILAND

Swaziland is a small, landlocked country in Southern Africa and is located between South Africa, on the

southern, western and northern side and Mozambique on the eastern side. The map of Swaziland is shown in Figure 1. On the western side of the country is the Highveld. The Lubombo plateau lies on the eastern side whilst the Middleveld and Lowveld lie between the Highveld and the Lubombo plateau. The areas of interest in this study, in connection with solar radiation, are Big Bend and Mhlume, both of which lie in the Lowveld, Matsapha (Middleveld) and Mbabane (Highveld). The altitude, latitude and longitude in the various locations are shown in Table 1. The country consists of four seasons, namely, spring (September-October), summer (November-February), autumn (March-May), and winter (June-August).

There are 11 weather stations in Swaziland, but solar radiation levels are recorded in only one, that is in Mhlume. However, daily maximum and minimum temperatures are routinely measured in all the weather stations. In this work, we use the solar radiation data from

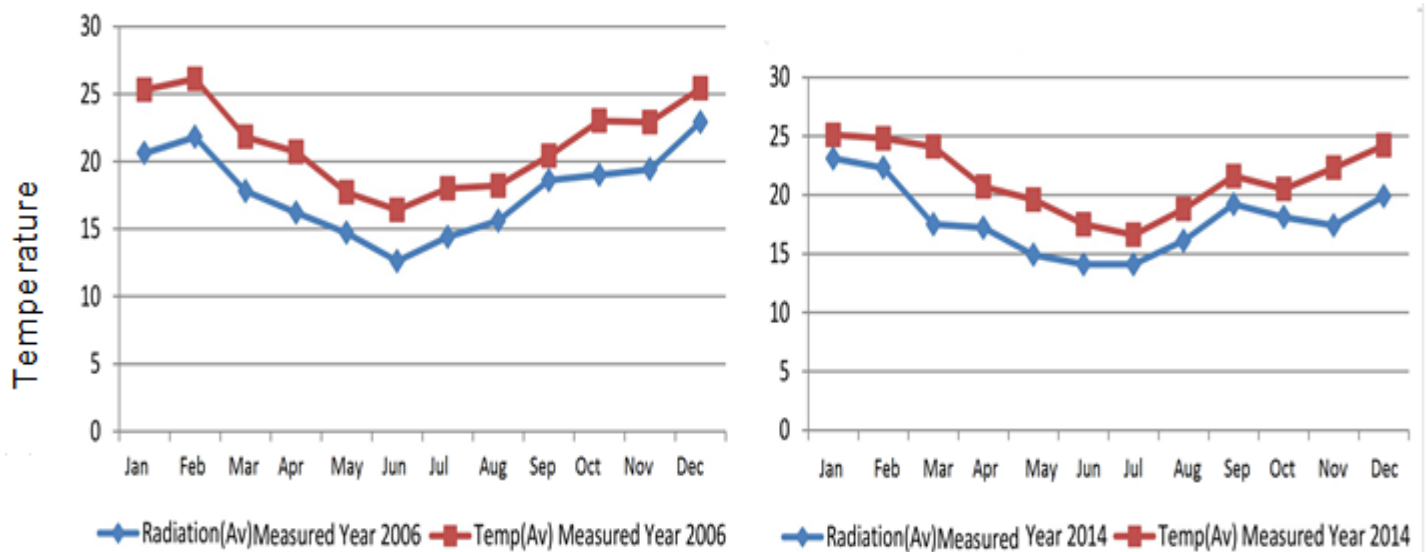


Figure 2. Monthly average solar radiation [MJ/m<sup>2</sup>] and air temperature (°C) in Mhlume.

Mhlume as a reference to develop and calibrate two mathematical models that define solar radiation as a function of temperature. The data is for the year 2004 to 2014.

Figure 2 shows that monthly average solar radiation levels at Mhlume are correlated with the monthly average temperature values. Maximum radiation levels were recorded between December and February, during the hottest season, and the lowest solar radiation levels were recorded between May and August, during the coldest season. Generally, the magnitude of the observed solar radiation is proportional to the observed average temperature.

**AIR TEMPERATURE BASED MODELS**

Given that the most commonly available climatological data in Swaziland is air-temperature, we consider air temperature based models to predict solar radiation at different locations within the country. We first consider that monthly average solar radiation  $H_{av}$  (MJ/m<sup>2</sup>) is a linear function of the monthly average temperature  $T_{av}$  (°C):

$$H_{av} = m_1 T_{av} + c_1 \tag{1}$$

Where  $T_{av} = (T_{max} + T_{min})/2$ ,  $T_{max}$  and  $T_{min}$  are the average daily maximum and minimum air temperature (°C) for a period of one month,  $m_1$  and  $c_1$  are empirical constants. The relationship expressed in Equation 1 or Model 1 is motivated by the observation in Figure 2 that the measured solar radiation values are proportional to the observed average temperatures, throughout the year. Previous studies have considered similar linear equations to predict solar radiation, for example, the classical Angstrom model (Angstrom, 1924) assumes that the magnitude of solar radiation is

proportional to sunshine hours (Angstrom, 1924; Meza and Varas, 2000; Liu et al., 2012; and Yakubu and Medugu, 2012).

Most temperature-based models in the literature (Meza and Varas, 2000; Liu et al., 2012) assume that solar radiation is a function of the difference between daily maximum and minimum air temperature. This is based on the assumption that the difference generally indicates daily cloudiness. Clear skies corresponds to higher solar radiations levels at the earth surface and cloudy skies corresponds to lower solar radiation levels. In this work, we compare the results of Equation 1 with the classical model of Hargreaves and Samani (1982) that assumes that:

$$H_{av} = m_2 H_0 \sqrt{T_{max} - T_{min}} \tag{2}$$

where  $H_0$  represents extra-terrestrial radiation and  $m_2$  is an empirical constant that usually ranges from 0.15 to 0.19, depending on whether the location has an arid or a coastal climate (Allen, 1997). The extra-terrestrial solar radiation,  $H_0$  is a function of latitude and can be easily evaluated or obtained in the literature (Duffie and Beckman, 2013). As the solar radiation passes through the earth’s atmosphere, it is further modified by processes of scattering and absorption due to the presence of cloud and atmospheric particles. Hence, the solar radiation at the earth’s surface is always less than  $H_0$ .

**Evaluation of model parameters**

We evaluated the empirical constants for Models 1 and 2 using the measured data of monthly average solar radiation and monthly average temperature at Mhlume during the period 2004 to 2014. These parameters were calculated using the Marquardt-Levenberg algorithm for curve fitting in Gnuplot. The curve-fitting results are also shown graphically in Figure 3 and the best fits are described by  $m_1 = 1.02 \pm 0.08$ ,  $c_1 = -4.28 \pm 1$  and  $m_2 = 0.161 \pm 0.002$ . This means  $m_2$  corresponds to the 0.16 that is recommended for this model for locations with arid or semi-arid climates (Hargreaves, 1994; Allen, 1997).



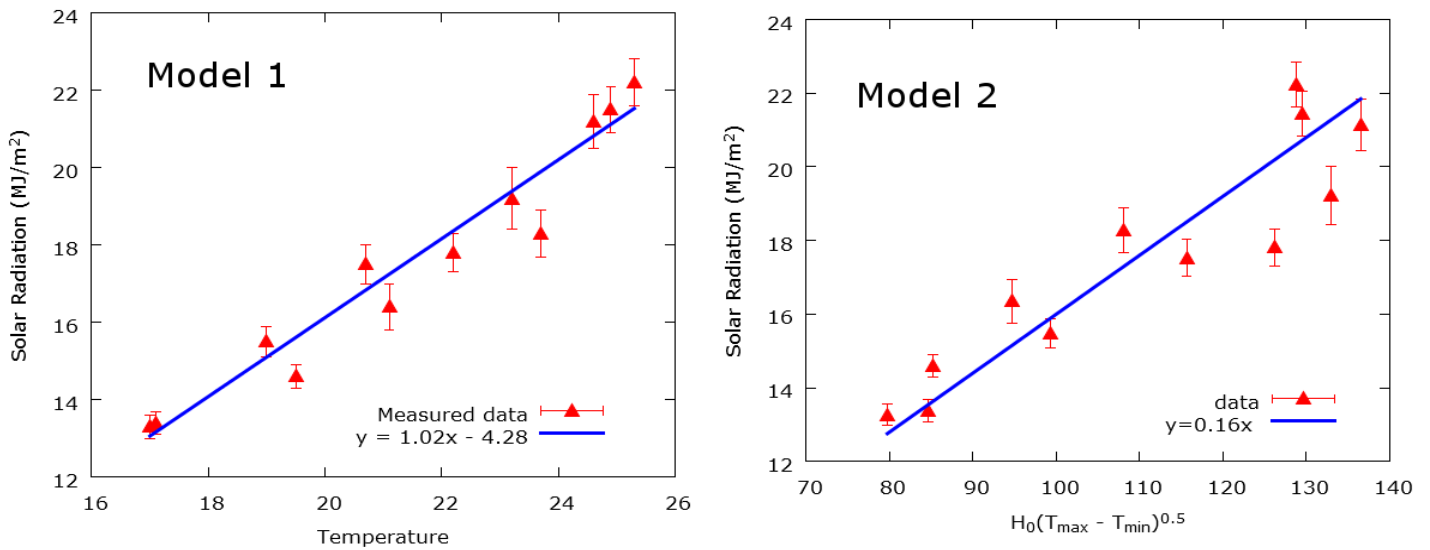


**Figure 3.** Evaluation of parameters of the two models. Monthly average solar radiation against monthly average temperatures from 2004 to 2014 in Mhlume (Model 1). Monthly average solar radiation against the square-root of the differences between the maximum and minimum monthly average temperatures from 2004 to 2014 in Mhlume (Model 2).

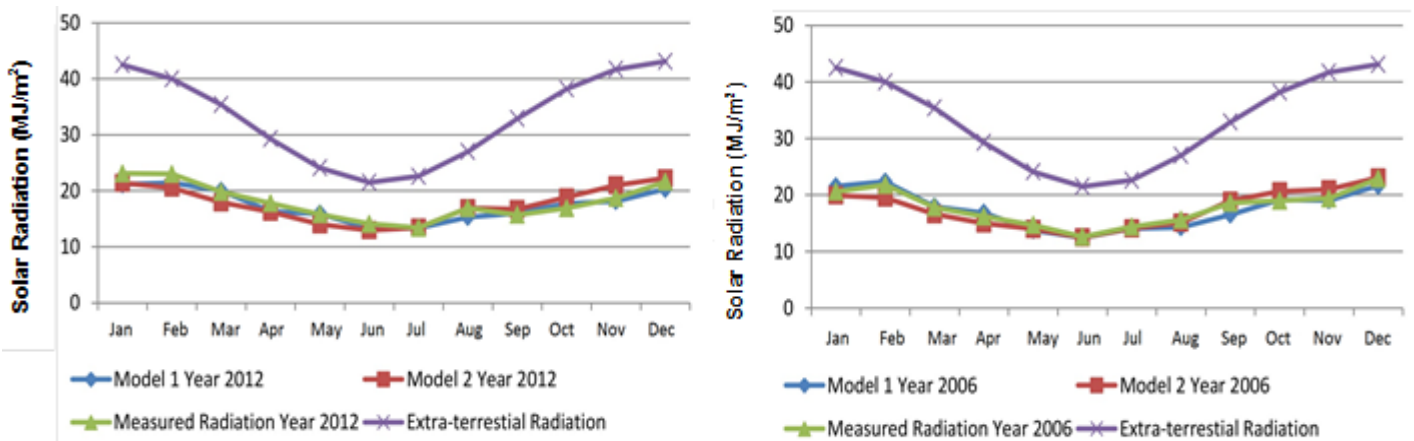


**Figure 4.** Monthly average solar radiation in Mhlume.

**RESULTS AND DISCUSSION**

**Performance of the models against measured data**

The calculated parameters were then utilized to estimate solar radiation levels for each year during the period between 2004 and 2014. The estimated values were then compared with measured values. Figure 4 shows a sample of these results and both models predict values that are consistent with the observed data. The extra-terrestrial solar radiation reaching Swaziland or regions located at the latitude 26.00°S is also given in Figure 4. As expected,

the magnitude of the measured or estimated solar radiation is less than the extra-terrestrial solar radiation at the same location since gases and dusts in the atmosphere change the magnitude and spectral composition of the solar radiation that reaches the earth’s surface.

In addition, the performance of the models can be quantified by evaluating the root-mean-square-error (RMSE) and the mean-percentage-error (MPE). These are fundamental measures of accuracy in solar energy calculations (Saffaripour et al., 2013; Li et al., 2014, Sonmete et al., 2011; Okundamiya et al., 2016). They are, respectively defined as:

**Table 2.** Error analysis between estimated and measured solar radiation data in 2006 and 2012 at Mhlume.

Error measurement	Model 1		Model 2	
	Year 2006 data	Year 2012 data	Year 2006 data	Year 2012 data
RMSE	0.93	1.11	1.11	1.58
PME (%)	-1.94	-3.28	-1.60	-1.86

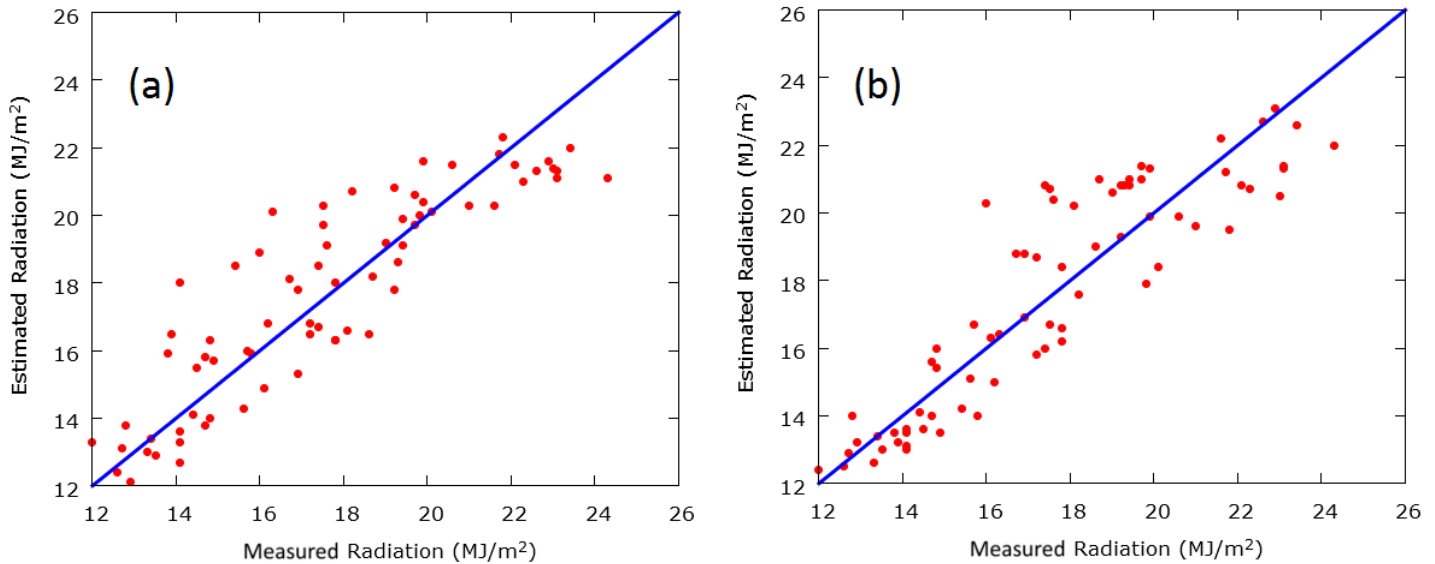


**Figure 5.** Comparison between measured and predicted monthly average solar radiation from year 2004 to 2014 in Mhlume. The estimates were obtained using Models 1 and 2 for (a) and (b), respectively.

$$RMSE = \left[ \frac{1}{n} \sum_{j=1}^n (H_{j,calc} - H_{j,meas})^2 \right]^{1/2} \tag{3}$$

and

$$MPE = \frac{1}{n} \sum_{j=1}^n \left( \frac{H_{j,calc} - H_{j,meas}}{H_{j,meas}} \right) \times 100\% \tag{4}$$

where  $n = 12$  is the number of data pairs,  $H_{j,calc}$  is the  $j$ -th calculated value and  $H_{j,meas}$  is the  $j$ -th measured value. Both models give an absolute MPE that is less than five percent, as shown in Table 2 which is considered acceptable in scientific calculations. Model 1 was found to give a lower value of RMSE, an indication of a better performance.

The behavior of the two models is further explored through a scatter plot of the estimated data against the measured data collected for over a decade from 2002 to

2014. Figure 5 shows that both models are consistent with the measured data over this period.

### Prediction of solar radiations in other locations

This research utilized the two models with their coefficient calibrated with the measured solar radiation data from Mhlume to estimate monthly average solar radiation levels at Big Bend, Matsapha, and Mbabane. The results are shown in Figure 6 for the year 2012. Both models give consistent results for Mhlume and Matsapha. Model 2 predicts slightly higher radiation levels than Model 1 for Mbabane. The predictions from the two models were then explored over longer periods, using air-temperature data collected between the years 2002 and 2013. The results are given in scatter plot in Figure 7 for the four locations. These results show that both models are consistent in all the locations except in Mbabane, where Model 1 generally predicts lower values than Model 2. This could be due to the fact that the altitude of Mbabane is higher than that of Mhlume by one order of magnitude (Table 1). Given that the value of  $m_2$  is within the recommended

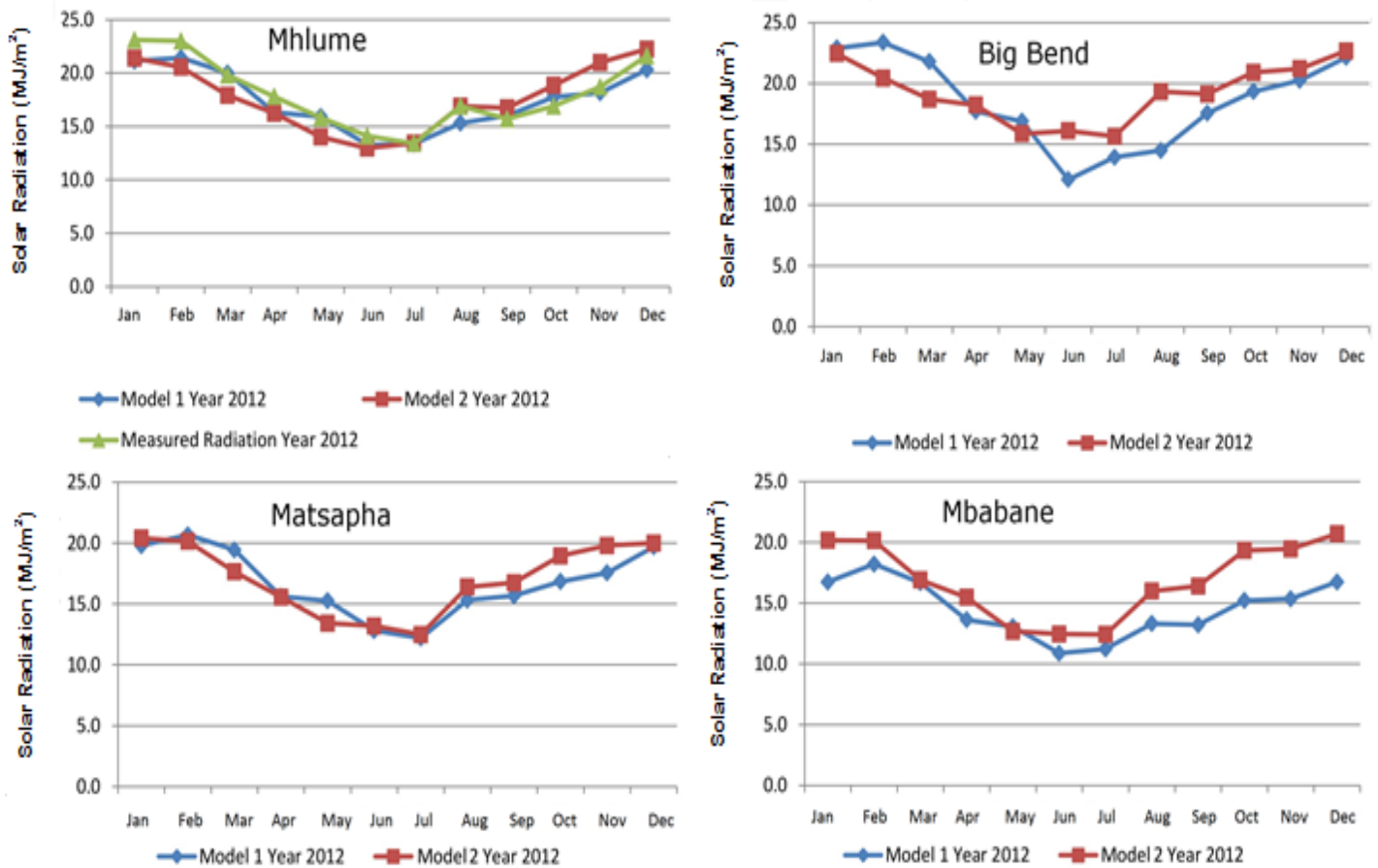


**Figure 6.** Estimated monthly average solar radiation in four different regions in Swaziland: Mhlume, Big-Bend, Matsapha, and Mbabane. Mhlume also includes measured data.

range for inland regions (Allen, 1997), Model 1 parameters need to be correctly readjusted for Mbabane.

**Conclusions**

Air-temperature based models for estimating solar radiation are useful for quantifying solar radiation levels in different locations around the world because they are based on commonly available meteorological data. In this study, a simple linear model that uses average monthly average air temperatures and the classical Hargreaves-Samani model (Equation 2) are shown to accurately predict solar radiation levels at Mhlume in Swaziland with an acceptable mean percentage error. The parameter of the Hargreaves-Samani Model calibrated with measured data from Mhlume is consistent with the value of 0.16 that was recommended by Heagreaves (1994) for inland regions.

For other locations within Swaziland with a slight

variation in climatic conditions from Mhlume, the same model parameters can be applied to predict their solar radiation levels. In this regard, we have found that the two models produce consistent results for two locations: Matsapha and Big Bend. However for the third location, Mbabane, which has a wider variation in climatic conditions than Mhlume, the models do not produce consistent results and therefore there is a need to correctly adjust the model parameters for Mbabane or similar regions.

Over the past decade, there has been a growing interest in the harnessing of solar energy in Swaziland; mainly using photovoltaic modules to reduce the amount of energy that is imported from neighboring countries. Currently, there is a 100 kW pilot solar farm that is operating in the Lubombo region and there is plan to set up an 850 kW solar plant at a location between Mhlume and Big Bend. Estimation of solar radiation using air-temperature data will therefore assist in the development of the solar energy industry in the country.

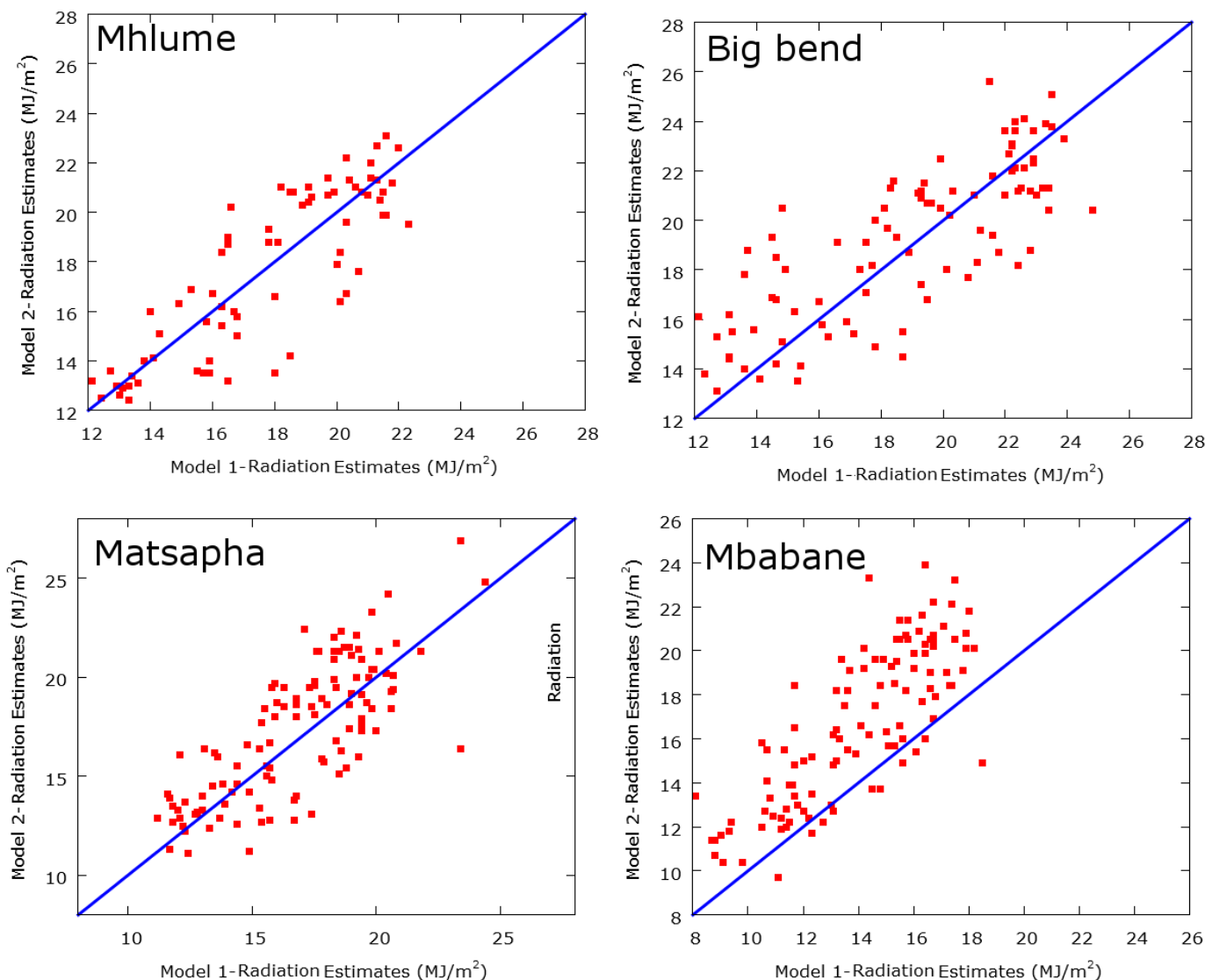


**Figure 7.** Comparison between estimated average solar radiation for year between 2002 and 2013 in Big Bend, Matsapha, Mbabane, and for years between 2004 and 2013 in Mhlume.

**CONFLICT OF INTERESTS**

The authors have not declared any conflict of interests.

**ACKNOWLEDGEMENTS**

The authors are grateful to the Royal Swaziland Sugar Corporation, Department of Geography, Environmental Science and Planning at the University of Swaziland (UNISWA), and the Swaziland Meteorological Services Department for providing the data used in this work. The authors also acknowledge the valuable suggestions from Dr. W. H. Liao of the Department of Physics (UNISWA).

**REFERENCES**

Allen RG (1997). Self-calibrating method for estimating solar radiation from air temperature. *J. Hydrol. Eng.* 2(2):56-67.  
 Angstrom A (1924). Solar and terrestrial radiation. *Q. J. R. Meteorol. Soc.* 50: 121-126.  
 Bajpai U, Singh K (2009). Estimation of instant solar radiation by using instant temperature. *Acta Montanistica Slovaca* 14(1):189-196.  
 Bristow KL, Campbell GS (1984). On the relationship between incoming solar radiation and daily maximum and minimum temperature. *Agric. For. Meteorol.* 31:159-166.  
 Chegaar M, Lamri A, Chibani A (1998). Estimating global solar radiation using sunshine hours. *Rev. Energ. Ren. : Physique Energetique* pp. 7-11.  
 Datta D, Datta BK, (2013). Empirical model for the estimation of global solar radiation in Dhaka, Bangladesh. *IJRET* 2(11):649-653.  
 Dos Santos CM, De Souza JL, Ferreira-Junior RA, Tiba C, de Melo RO,

- Lyra GB, Teodoro I, Lyra GB, Lemes MAM (2014). Modelling global solar irradiation using air temperature for Alagoas state, northeastern Brazil. *Energy* 2014:1-11.
- Duffie JA, Beckman WA (2013). *Solar Engineering of Thermal Processes*, John Wiley, New Jersey.
- Hargreaves GH (1994). Simplified coefficients for estimating monthly solar radiation in North America and Europe. Dept. Biol. And Irrig. Engrg. Utah State Univ., Logan, Utah.
- Hargreaves GH, Samani ZA (1982). Estimating potential evapotranspiration. *J. Irrig. Drain. Engr.* 108:223-230.
- Kostic R, Mikulovic J (2017). The empirical models for estimating solar insolation in Serbia by using meteorological data on cloudiness. *Renew. Energy* 114:1281-11293.
- Li H, Cao F, Bu X, Zhao L (2014a). Models for calculating daily global solar radiation from air temperature in humid regions—a case study. *Environ. Prog. Sustain. Energy* 34(2):595-599.
- Li H, Cao F, Wang X, Ma WA (2014b). A temperature-based model for estimating monthly average daily global solar radiation in China. *Sci. World J.* 2014:128754, 1-9.
- Liu J, Liu J, Linderholm HW, Chen D, Yu Q, Wu D, Haginoya S (2012). Observation and calculation of solar radiation on the Tibetan Plateau. *Energ. Convers. Manage.* 57:23-32.
- Meza F, Varas E (2000). Estimation of mean monthly solar global radiation as a function of temperature. *Agric. For. Meteor.* 100:231-241.
- Okundamiya MS, Emagbetere JO, Ogunjor EA (2016). Evaluation of various global solar radiation models for Nigeria. *Int. J. Green Energy* 13(5): 505-512.
- Saffaripour MH, Mehrabian MA, Bazargan H (2013). Predicting solar radiation fluxes for solar energy system applications. *Int. J. Environ. Sci. Technol.* 10:761-768.
- Sonmete MH, Ertekin C, Menges HO, Haciseferogullari H, Evrendilek F (2011). Assessing monthly average solar radiation models: a comparative case study in Turkey. *Environ. Monit. Assess.* 175:251-277.
- Umoh MD, Udo SO, Udoakah YO (2014). Estimating global solar radiation on horizontal surface from sunshine hours over Port Harcourt, Nigeria. *J. Electr. Electron. Eng. Res.* 6(1):1-5.
- Yakubu D, Medugu DW (2012). Relationship between the global solar radiation and the sunshine duration in Abuja, Nigeria. *Ozean J. Appl. Sci.* 5(3):221-228.
- Yang K, Koike T, Ye B (2006). Improving estimation of hourly, daily, and monthly solar radiation by importing global data sets. *Agric. For. Met.* 137:43-55.

*Full Length Research Paper*

# A study of semi-annual variation of residual geomagnetic field and its association with solar and geomagnetic activity

Egba Ibeabuchi G.<sup>1\*</sup>, Kalu Florence D.<sup>1</sup>, Okwesili Agatha N.<sup>1</sup> and Okpala Kingsley C.<sup>1,2</sup>

<sup>1</sup>Department of Physics and Astronomy, University of Nigeria, Nsukka, Enugu State, Nigeria.

<sup>2</sup>Department of Physics, Benue State University, Makurdi, Benue State, Nigeria.

Received 26 July, 2017; Accepted 22 September, 2017

The semi-annual variation of the residual H and Z components of geomagnetic field was studied by analyzing magnetograms with sixty-one years data. Mean monthly residual H- and Z-component field ( $H_{diff}$  and  $Z_{diff}$ ) variations were computed using appropriate technique. Semi-annual variation exhibited  $H_{diff}$  peaks in the equinoxes, which for low latitudes, was higher during March/April than in September/October. In the mid and high latitude stations also,  $H_{diff}$  exhibited clear semi-annual variation albeit with less intensity during the equinoxes. Mid latitude broad peaks in the said variation suggest longitudinal asymmetric contributions to the ring currents.  $Z_{diff}$  in all the latitudes exhibited greater asymmetry in its distribution in comparison with  $H_{diff}$ .  $Z_{diff}$  variation was largest in the high latitude regions, showing strong solar activity dependence. It is suggested that asymmetric component of the ionospheric coupling to the magnetospheric current may be responsible for the observed irregularities in the low- and mid-latitude  $Z_{diff}$  semi-annual variation, while the East-West and West-East currents in the auroral oval region may be modulating the ring current effect on residual field at high latitudes.

**Key words:** Geomagnetic field, magnetograms, H and Z components.

## INTRODUCTION

Solar activity refers to the natural phenomena occurring within the magnetically heated outer atmospheres in the sun throughout the solar cycle. This activity takes the form of solar wind acceleration, flux emergence, light and energy particles released from the sun such as solar flares, coronal mass ejection or solar eruptions, and coronal heating; as well as sunspots which are one of the most commonly noticed forms of solar activity.

Geomagnetic activity can be separated into auroral magnetic activity and magnetic substorms. Auroral magnetic activity involves the enhanced auroral light displays, currents, and magnetic perturbation associated with times when favorable magnetic coupling causes enhanced plasma flows down the cusp field lines into the auroral regions. Magnetic substorms occur, however, when the magnetosphere is loaded with excess energy

\*Corresponding author. E-mail: [abuchiegbaexplore@gmail.com](mailto:abuchiegbaexplore@gmail.com).

during a period with sustained southwards interplanetary magnetic field (IMF-Bz). These geomagnetic activities constitute a major part of the monthly disturbances in the geomagnetic field and they are generally quantified by the geomagnetic storm time index – Dst, and the average planetary disturbance index – Ap. The Ap index represents the daily intensity of planetary magnetic activity as seen at sub-auroral latitudes, while the Dst measures the ring-current magnetic field based on hourly average values of the H component recorded at four low latitude observatories after subtracting the average square and the permanent field from the disturbed magnetic field (Fares Saba et al., 1997).

The measured magnetic field on the surface of the earth is generally linked to three sources: i) main field which is generated by hydrodynamic dynamo system in the Earth's core, ii) current systems in the ionosphere and magnetosphere, and iii) magnetized rocks in the Earth's lithosphere. The magnetospheric and ionospheric currents are usually regarded as the external magnetic field components of the measured field at the surface of the Earth. These external fields are also responsible for induction currents at the mantle of the Earth which further modify the measured field.

Many authors have attempted to separate the symmetric and asymmetric contributions to the magnetospheric ring current using spherical harmonic analysis (Banks, 1969; Xu et al., 2015), wavelet analysis (Mendes et al., 2005; Xu et al., 2009), and ion density variations (Daglis and Axford, 1996). Most of these studies have investigated the symmetric ring current using the well-known signature of Dst during geomagnetic storms. The ring current is an electric current carried by charged particles trapped in the magnetosphere. It is caused by the longitudinal drift of energetic particles. The ring current provides the geomagnetic conditions for magnetic storms to settle down (Mendes et al., 2005). It dominates at middle and low latitudes, and a system of ionospheric electrojet currents flowing in the auroral oval dominates at higher latitudes. The ring current is ever present and its long term structure is detectable in the monthly mean geomagnetic field essentially leading to weaker mean geomagnetic field during disturbed times and stronger field during quiet times. Forbush and Beach (1967) first introduced the concept that departures of quiet and disturbed X component of the geomagnetic field ( $X_{RC}(Q)$  and  $X_{RC}(D)$ ), respectively) maintain a fixed ratio to each other throughout the solar cycle such that;

$$X_{RC}(Q) = k * X_{RC}(D) = \frac{k}{1 - k} (X_{RC}(D) - X_{RC}(Q)) \quad (1)$$

Thus by equating  $X_{RC}(D) - X_{RC}(Q)$  with  $X(D - Q)$  the absolute ring current field can be estimated from observatory data, once an appropriate value for k is found. Furthermore it was suggested that k is a universal constant. This implies that the geometry of the ring current field is the same

throughout the solar cycle and the same on quiet days and disturbed days. The difference measures the absolute strength of the ring current and should define the Dst connection to monthly and annual means. In the present study, Equation 1 is applied and the North component (X) replaced with H-component and monthly mean computed for all days to reflect mean strength of the ring current for the particular month.

The objectives of this study are to investigate the variation of the residual field on seasonal and annual scales in low-, mid- and high latitude stations and examine them for indications of possible anomalous behavior.

## DATA AND ANALYSIS

The magnetic data used for this study was obtained from 10 observatories within the northern hemisphere, cutting across low-, mid- and high-latitudes. Two of the stations (Sanjuan, and Honolulu) were used in computing Dst (disturbance storm time) index. Dst index is a function of the current inside and on the boundary of the magnetosphere, and it measures the ring-current magnetic field based on hourly average values of the H component. The data was originally in hourly time resolution and was converted to daily values covering the year 1950 to 2010 (61 years). Data presented in X and Y were converted to H since the interest is in H and Z components, where X, Y, H and Z represent northerly intensity, easterly intensity, horizontal intensity and vertical intensity, respectively of the geomagnetic field. The geomagnetic field data is provided by the world data center (WDC) for geomagnetism Kyoto, Japan (Table 1). The daily Dst, average planetary disturbance (Ap) index, solar wind (SW) velocity and density, sunspots number (SSN) are provided by OMNIWeb. Data was selected based on the criterion of length and continuity of series of the geomagnetic field components. Monthly mean from all days in a given month for H-component and Z-component denoted by  $H_{all}$  and  $Z_{all}$  was computed as:

$$H_{all} = \frac{\sum_{i=1}^{n_0} H_i}{n_0} \quad (2a)$$

$$Z_{all} = \frac{\sum_{i=1}^{n_0} Z_i}{n_0} \quad (2b)$$

$H_i$  and  $Z_i$  are the respective H and Z component of the  $i$ th day of the month,  $n_0$  = no of days depending on the month of the year. The monthly mean value for the five quietest days of a given month was computed as:

$$H_{sq} = \frac{\sum_{j=1}^x H_j}{x} \quad (3a)$$

$$Z_{sq} = \frac{\sum_{j=1}^x Z_j}{x} \quad (3b)$$

$H_j$  and  $Z_j$  are the respective H and Z component of the corresponding  $j$ th quietest day of the month,  $x = 5$  days. The residual field for H and Z ( $H_{diff}$  and  $Z_{diff}$ ) is obtained as the difference between the monthly mean from all days ( $H_{all}$  and  $Z_{all}$ ) and the monthly mean of the international quietest days ( $H_{sq}$  and  $Z_{sq}$ ), that is:

$$H_{diff} = H_{all} - H_{sq} \quad (4a)$$

**Table 1.** Geomagnetic observatories showing geomagnetic and geographic location of stations.

Station Name/Code	Geographic Lat.	Geographic Long.	Geomagnetic Lat.	Geomagnetic Long.
<b>Low latitude Stations</b>				
Alibag/ABG	18.64N	72.08E	9.50N	144.50E
Guam/GUA	13.60N	144.9E	4.00N	212.9E
Honolulu/HON	21.32N	158.00W	21.30N	91.61W
San Juan/SJN	18.11N	66.15W	29.15N	5.02E
<b>Mid latitude Stations</b>				
Fredericksburg/FRD	38.20N	77.37W	49.12N	7.97W
Hurbanovo/HRB	47.87N	18.19E	46.69N	101.06E
Neimegk/NGK	52.07N	12.68E	51.77N	97.76E
<b>High Latitude</b>				
College/CMO	64.87N	147.87W	64.90N	101.16W
Eskdalemuir/ESK	55.32N	3.20W	57.92N	84.09E
Fort Churchill/FCC	58.78N	94.09W	68.47N	34.21W

Source: World Data Center for geomagnetism Kyoto, Japan.

**Table 2a.** Correlation coefficients between H<sub>diff</sub> and solar/geomagnetic activity indices for all stations.

Activity index	Monthly H <sub>diff</sub>									
	Low lat. Stations				Mid lat. Stations			High lat. Stations		
	ABG	GUA	HON	SJN	FRD	HRB	NGK	CMO	ESK	FCC
Dst	0.74	0.72	0.68	0.69	0.71	0.70	0.71	0.61	0.66	-0.02
Dst*	0.74	0.71	0.67	0.68	0.71	0.67	0.71	0.61	0.66	-0.02
SSN	0.29	0.23	0.22	0.23	0.17	0.21	0.18	-0.02	0.08	-0.07
Ap	0.31	0.33	0.31	0.30	0.28	0.12	0.28	0.30	0.23	-0.08
Dst <sub>all-sq</sub>	0.96	0.93	0.94	0.94	0.92	0.91	0.90	0.61	0.83	0.06
Dst <sub>all-sq</sub> *	0.85	0.80	0.80	0.82	0.79	0.76	0.77	0.53	0.70	-0.02

**Table 2b.** Correlation coefficients between Z<sub>diff</sub> and solar/geomagnetic activity for all stations.

Activity index	Monthly Z <sub>diff</sub>									
	Low lat. Stations				Mid lat. Stations			High lat. Stations		
	ABG	GUA	HON	SJN	FRD	HRB	NGK	CMO	ESK	FCC
Dst	-0.08	0.02	-0.34	-0.14	-0.31	-0.49	-0.45	-0.44	-0.31	-0.33
Dst*	-0.08	0.02	-0.34	-0.14	-0.31	-0.48	-0.45	-0.44	-0.32	-0.33
SSN	0.05	-0.09	0.03	0.05	-0.11	-0.32	0.32	0.39	0.34	0.04
Ap	0.10	0.01	0.40	0.11	0.26	0.51	0.42	0.45	0.21	0.44
Dst <sub>all-sq</sub>	-0.22	0.03	-0.50	-0.16	-0.56	-0.77	-0.78	-0.51	-0.57	-0.41
Dst <sub>all-sq</sub> *	-0.14	-0.04	-0.41	-0.14	-0.48	-0.69	-0.68	-0.49	-0.49	-0.35

$$Z_{diff} = Z_{all} - Z_{sq} \quad (4b)$$

H<sub>diff</sub> and Z<sub>diff</sub> are the residual fields which measure the absolute strength of the ring current in addition to other external and internal sources of geomagnetic field (excluding the solar daily variation) for the month assuming that the ring current geometry does not change much over monthly scales.

The linear correlation coefficients between the monthly mean H<sub>diff</sub> and Z<sub>diff</sub> for all the stations and some solar (SSN)/geomagnetic (Dst, Ap) activity indices is shown in Tables 2a and 2b, respectively. The mean of the low, mid and high latitude stations were taken and plotted over the period of years of this study to obtain the semi-annual H<sub>diff</sub> and Z<sub>diff</sub> variations. These plots are shown in Figures 1, 2 and 3 respectively.



## RESULTS AND DISCUSSION

### Correlation analysis

A linear association was assumed between  $H_{diff}$  and solar activity. This is a fair assumption considering that both the annual and semi-annual variations are controlled by solar activity which in turn controls geomagnetic activity. Table 2a is the linear correlation coefficients for  $H_{diff}$  against solar (SSN) and geomagnetic (Dst and Ap) activity indices. For high latitude stations, the correlation is not as strong but is generally  $> 0.60$  for most high latitude sub-aurora stations except for FCC which is an aurora station. The correlation appears to be latitude dependent and could lead to a means of reproducing mid and low latitude fields from derived Dst measurements. The total contribution of the induced field is about 11 to 15% of the statistical association and this is observed in all the stations used in this study. These observations are consistent with wavelet and cross spectra analysis observations by Xu et al. (2009), suggesting that the slow-time varying component of the ring current are largely globally symmetric. The solar activity index (SSN) did not correlate well with the  $H_{diff}$  in all the stations used. This poor correlation may not be unconnected with the indirect solar forcing of the ring current leading to significant semi-annual variation in the geomagnetic activity with disturbance field at each station.

Correlation between  $Z_{diff}$  and  $Dst_{all-sq}$  for all stations was higher than that for  $Z_{diff}$  vs  $Dst^*_{all-sq}$  (Table 2). The low latitude stations ABG, GUA and SJN showed weak correlation ( $< 0.20$ ). This low latitude observation can be explained by the weak low latitude Z-component field when compared with the mid and high latitudes Z field. The symmetric ring current does not have a significant component in the Z axis but in the North-South direction. The  $Z_{diff}$  showed a weaker correlation with SSN when compared with the geomagnetic activity index in the mid-latitudes and high-latitudes. Variability in the high latitude is expected to depend on solar activity since more particles are injected into the open magnetic field in the auroral oval which significantly modifies the magnetic field measured there. The observed increase in  $Z_{diff}$  during the equinox is evidence of the enhanced westward polar electrojet during enhanced geomagnetic activity. The solar quiet day effect on the Dst-related magnetic variation is dominant in the mid latitude when compared with low and high latitude. Removing the induced field component however reduces this correlation in a nearly uniform manner for all the stations considered. The constantly negative correlation for all stations shows that the observations are consistent with an inverse relationship between the symmetric ring current and the main magnetic field.

### $H_{diff}$ and $Z_{diff}$ variation

The semi-annual residual field variation in the low

latitudes (obtained as the mean  $H_{diff}$  from the four low latitude stations (ABG, GUA, HON, SJN)) is shown in Figure 1a. There is a visible semi-annual peak around March/April and September/October which is similar to observations of earlier authors, for example, Wardinski and Manda (2006). The semi-annual variation is more prominent during years of solar maximum activity. For solar minimum years, the semi-annual peak is greater in March/April than in September/October. The usual prominent semi-annual peaks observed during solar maximum years was missing in the 1970 to 1971 peak, possibly connected with earlier reports of marked diminutions in sunspots and 2800 MHz flux which took place in 1970 and 1971, respectively, and were accompanied by concomitant decreases in flare-occurrence (Dodson and Hedeman, 1975).

The usual semi-annual variation observed in the H component is a little more complicated in the low latitude  $Z_{diff}$  as shown in Figure 1b. The  $Z_{diff}$  tend to exhibit positive values around March-April-May and September-October-November which is expected for a ring current flowing westward over the equator. The range of variation is between -4 to 5 nanotesla (nT). Solar-cycle variation is not very prominent even for periods of very high solar activity. This observation is likely a result of the dominance of the effect of geomagnetic activity on the Z component even though the statistical association between  $Z_{diff}$  and Dst (or  $Dst_{all-sq}$ ) is weak for most low latitude stations. The relative shift in the time of the equinoctial peaks is currently unexplained.

The mid latitude  $H_{diff}$  variations exhibited semi-annual peaks between February - April and September - November as shown in Figure 2a. The broad peaks suggest that longitudinal asymmetric contributions to the ring currents are dominant at the mid latitude. During the maximum and declining phase of all the solar cycle covered in this study and especially cycle 20 and 22, the semi-annual peaks are broad and generally spread into the adjacent maximums. This is an evidence that Dst-related disturbance is more symmetric in the response to the North-South migration of the ring current when compared to the fluctuating solar activity.

Variations in line with solar cycle were not observed in the mid latitude  $Z_{diff}$  (Figure 2b), except for the deep solar cycle minima in 1962 to 1965 and 2004 to 2008. The equinoctial peaks in April and October are spread toward earlier months and quite complicated by other current systems coupled to the ring current. A slightly greater peak value is observed around the equinoxes in the mid latitude when compared to the low latitudes  $Z_{diff}$ . The range of  $Z_{diff}$  variation is between -1nT and 7nT. Asymmetric sources are likely a significant component of the  $Z_{diff}$  variation. Mid latitude ionospheric current contributions to the semi-annual variation may be a leading candidate for the asymmetric source.

Semi-annual peaks were quite distinct and prominent in the high latitude, showing minimum Dst-related

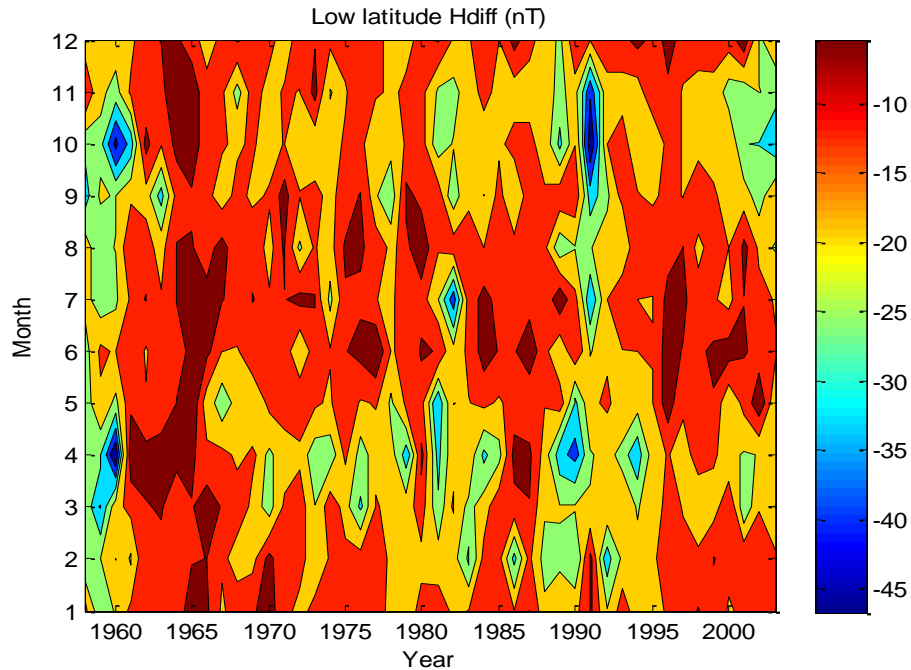


**Figure 1a.** Monthly  $H_{diff}$  for low latitude stations.

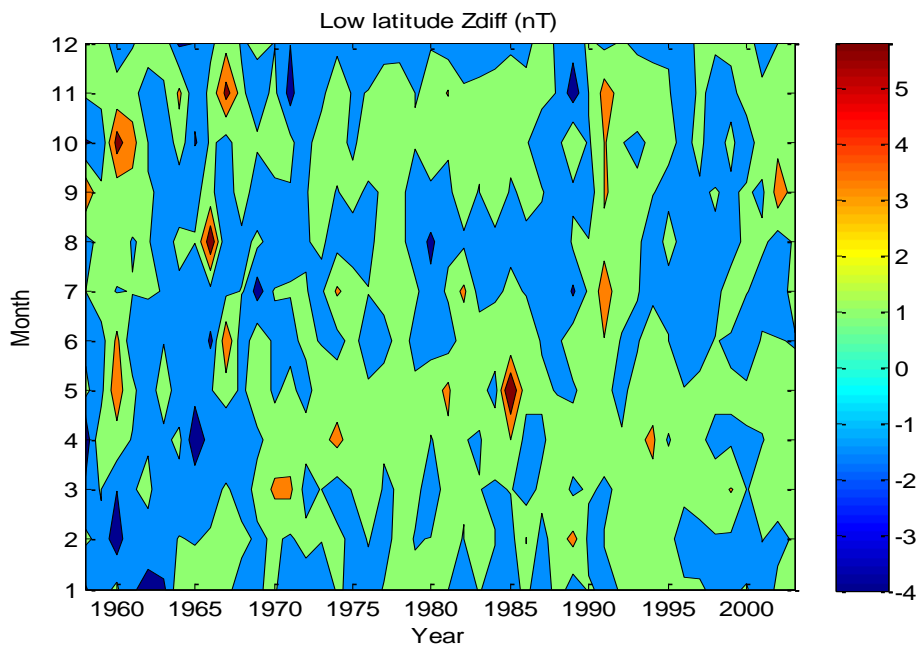


**Figure 1b.** Monthly  $Z_{diff}$  for low latitude stations.

disturbance  $H_{diff}$  in the summer months as shown in Figure 3a. The extended minimums of cycle 19 and 23 were evident in the plot. The Dst-related disturbance in this region may be enhanced by sub-storm Westward polar electrojet since the symmetric peaks in the March-

April and September-October are distinct irrespective of the usual presence of strong asymmetric component in the high latitudes. This observation supports the understanding that the partial ring current seems to develop and decay earlier than the symmetric ring

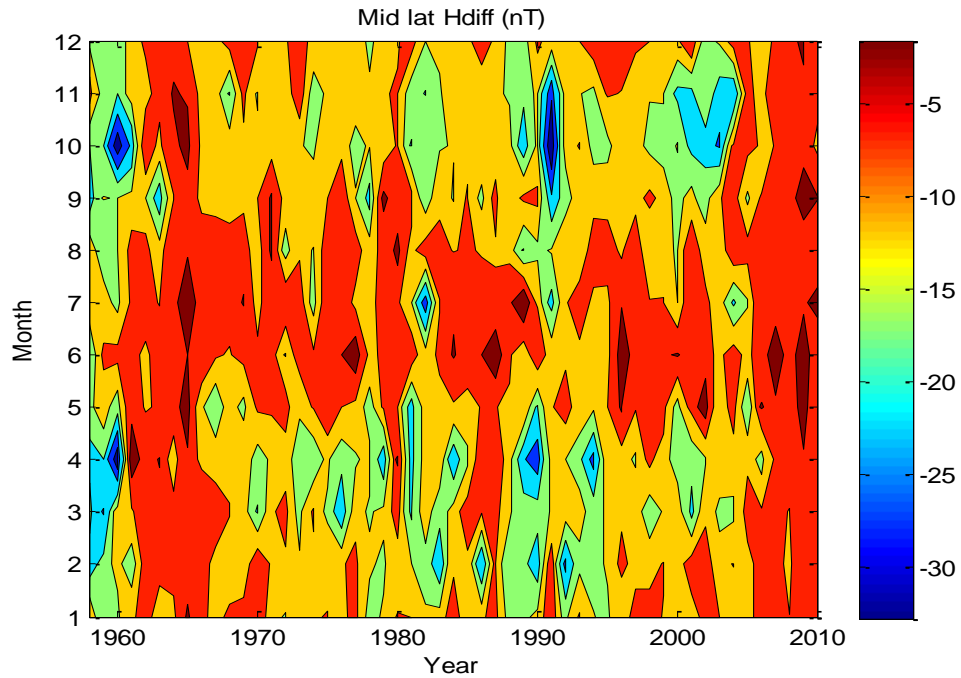


Figure 2a.  $H_{diff}$  variation using the mean of the mid latitude stations.

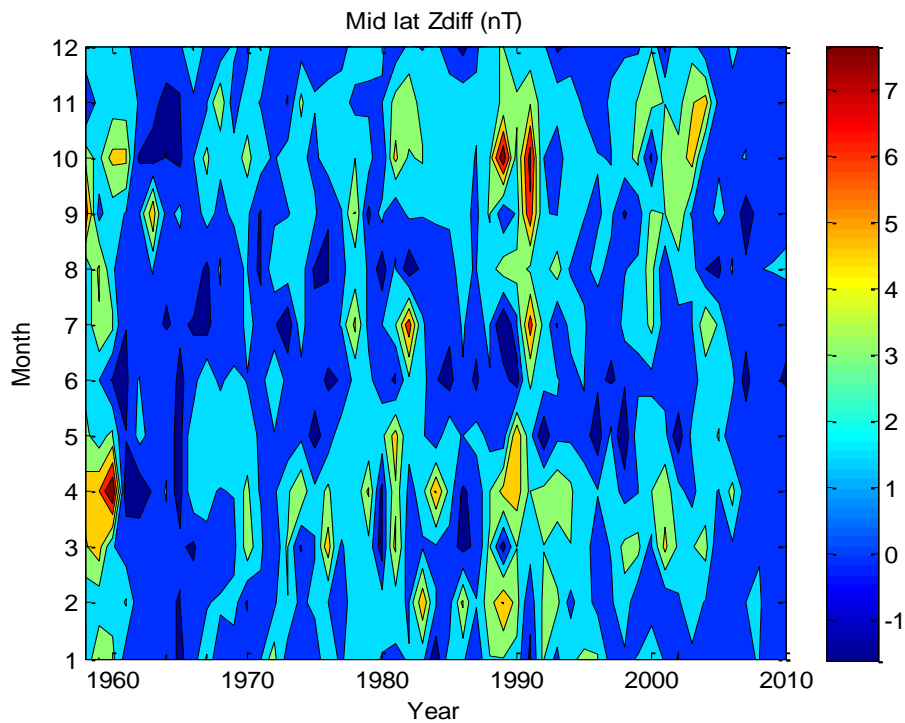
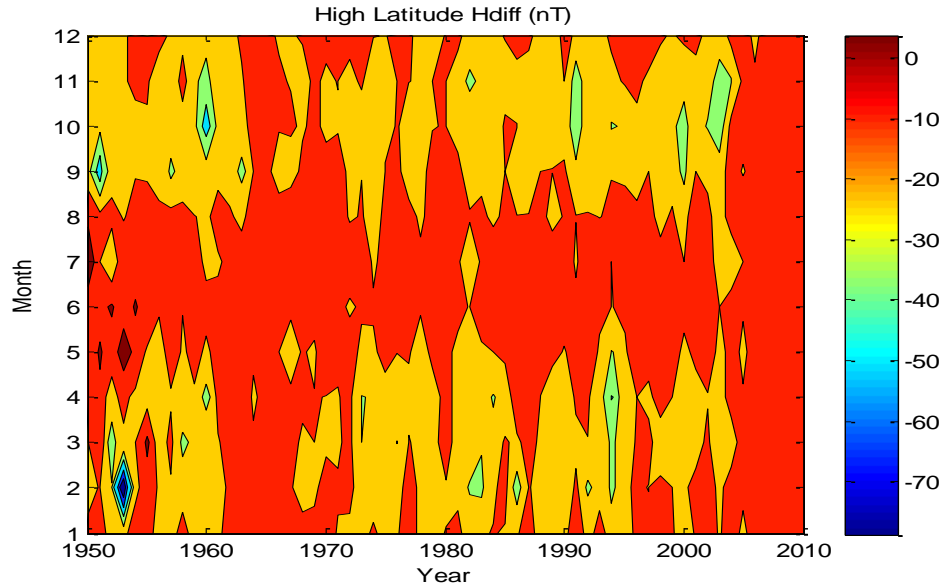


Figure 2b.  $Z_{diff}$  variation using the mean of the mid latitude stations.

current, which is responsible for the worldwide uniform decrease in  $H_{diff}$  observed in all the stations used in this study independent of latitude.

High latitude  $Z_{diff}$  variations (Figure 3b) show very significant solar cycle dependence. Positive  $Z_{diff}$  occur during solar maximum years while negative  $Z_{diff}$  occur



**Figure 3a.**  $H_{diff}$  variation using the mean of the high latitude stations.

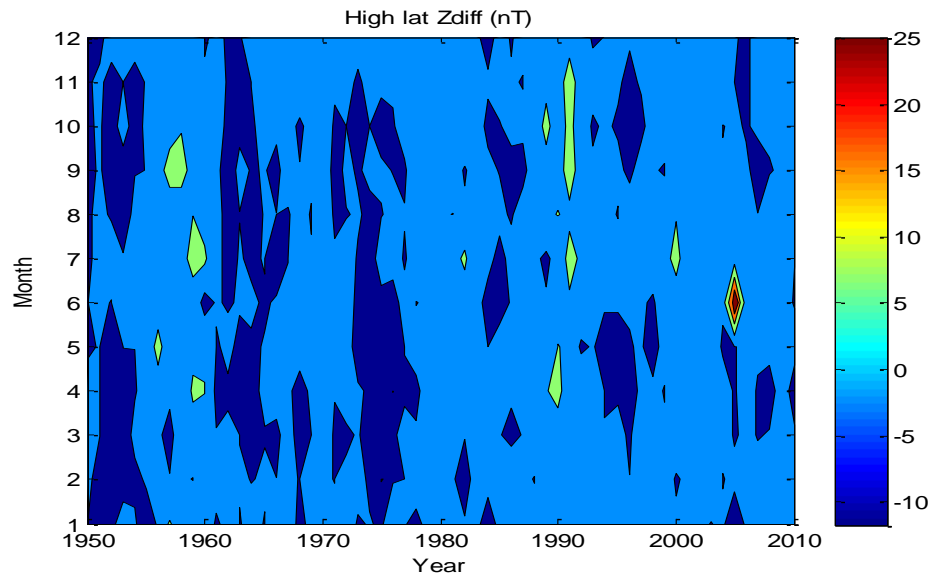


**Figure 3b.**  $Z_{diff}$  variation using the mean of the high latitude stations.

during the period of minimum solar activity. The range of the variation in  $Z_{diff}$  is from  $-10\text{nT}$  to  $25\text{nT}$ . The semi-annual variation is not very clear in this region. The high values of  $Z_{diff}$  are a confirmation of the Westward current dominance observed in the  $H_{diff}$  plot.

## Conclusion

The present study showed that the internal induced field

contribution to the Dst-related disturbance is significant and quite symmetric in the low- and mid-latitudes, and weaker in the high-latitude.  $Dst_{all-sq}^*$  may be potentially useful for reproducing the magnetic field in mid- and low-latitudes.  $H_{diff}$  semi-annual variation in the low latitude is more prominent during years of maximum solar activity. For solar minimum years, the semiannual peak is slightly greater in March/April than in September/October. The  $H_{diff}$  enhancements observed in the mid- and high-latitude during March / April and September / October were

generally more intense than those observed in the low latitudes.  $Z_{diff}$  is largest in the high latitude and showed a tendency of being more negative during periods of solar minimum as compared with the periods of solar maximum. The westward auroral current compliments the ring current during periods of high solar activity leading to a positive  $Z_{diff}$  and an observable semi-annual variation in the  $H_{diff}$ . Other asymmetric sources (like the field aligned current) and regional tendencies in conductivity profiles may also be contributing to this variability.

## CONFLICT OF INTERESTS

The authors have not declared any conflict of interests.

## REFERENCES

- Banks RJ (1969). Geomagnetic variations and electrical conductivity of the upper mantle. *Geophys. J. R. astr. Soc.* 17:457-487.
- Daglis IA, Axford WI (1996). Fast ionospheric response to enhanced activity in geospace: ion feeding of the inner magnetotail. *J. Geophys. Res.* 101: 5047-5065.
- Dodson HW, Hedeman ER (1975). Comments on the course of solar activity during the declining phase of solar cycle 20 (1970-74). *Sol. Phy.* 42(1):121-130.
- Fares Saba MM, Gonzalez WD, Gonzalez AI (1997). Relationship between the AE, Ap and Dst indices near solar minimum (1974) and at solar maximum (1979). *Ann. Geophys.* 15:1265-1270.
- Forbush SE, Beach L (1967). The absolute geomagnetic field of the equatorial ring current. *Carnegie Institution Yearbook* 65:28-36.
- Mendes O, Domingues MO, Da-costa C, De-Gonzalez ALC (2005). Wavelet Analysis Applied to magnetograms: Singularity detections related to geomagnetic storms. *J. Atmos. Sol. Terrest. Phys.* 67(17):1827-1836.
- Wardinski I, Manda M (2006). Annual and semi-annual variations of the geomagnetic field components analysed by the multi-taper method. *Earth Planets Space* 58:785-791.
- Xu D, Chen H, Gao M (2015). Observed geomagnetic induction effect on Dst-related magnetic observations under different disturbance intensities of the magnetospheric ring current. *Earth Planets Space.* 67:15.
- Xu Z, Zhu L, Sojka J (2009). Wavelet cross-spectrum analysis of the ring current using magnetic records from multiple low latitude stations. *J. Geophys. Res.* 114:A5.

*Full Length Research Paper*

# Radioactivity in building materials in Saudi Arabia: An overview of experimental method and Monte Carlo N-Particle (MCNP) calculation

H. Alshammari<sup>1\*</sup>, Abdulrahman Alghamdi<sup>1</sup> and Ahmed Algammidi<sup>2</sup>

<sup>1</sup>King Abdulaziz City for Science and Technology, Riyadh 11442, P. O. Box 6086, Saudi Arabia.

<sup>2</sup>Department of Chemistry, King Saud University, Riyadh Saudi Arabia.

Received 28 April, 2017; Accepted 22 September, 2017

The aims of this work were clearly to assess the norms of radiation protection for building residents against natural radioactivity. This was done through measurement of natural radioactivity in building materials using gamma ray spectrometer. The annual effective dose (HR) linked to natural radioactivity was computed to estimate the radiation hazard in building materials. Obtained concentrations of these natural radionuclides and the calculated radiation hazard were compared with the national recommended values by natural limits by the Saudi standard code for radiation protection. The findings in this work of natural radioactivity levels were below the acceptable limits of 1 mSv/year which were found near the border of these limits. Therefore, it was found that the building materials may be safe to be used as construction materials. The annual effective doses were  $0.8 \pm 0.2$  mSv/year for ceramics,  $0.08 \pm 0.02$  mSv/year for adhesives,  $0.6 \pm 0.28$  mSv/year for porcelains,  $0.2 \pm 0.1$  mSv/year for marbles,  $0.01 \pm 0.01$  mSv/year for paints, and 0.015 mSv/year for gypsum materials. The obtained results were compared with Monte Carlo N-Particle (MCNP) simulation. MCNP simulation was formulated to calculate the indoor gamma dose rate from the activity levels of the building materials which can take sample into very precise level. This computation was utilized to assess the uncertainty in the estimates. The results of MCNP were presented and an evaluation of the reported data shortly discussed. The radiation experimental values are in good agreement with the MCNP values, indicating that the obtained results are precise. Materials covered in the study are marbles, ceramics, adhesives, porcelain, paints, and locally produced cements.

**Key words:** Radioactivity, building materials, gamma ray spectrometer.

## INTRODUCTION

Natural gamma radiations of indoor exposure owing to building materials, primitively quantified in building materials, is regarded as more significant than outdoor

exposure. Natural radionuclides are always present in building materials but in various concentrations. Building materials often contain thorium and uranium decay series

\*Corresponding author. E-mail: hshamari@kacst.edu.sa.

**Table 1.** The HPGe specifications.

Geometry	Co-axial open end closed end facing window
Diameter	74.7 mm
Length	92.9 mm
Active area window	11.6 mm
Operating voltage	4500V
Leakage current	0.01A
Amplifier gain	50
Amplifier ne	30-40
Pulse time	6 $\mu$ s

radionuclides; therefore radiation exposure arises mostly from Th<sup>-232</sup>, U<sup>-238</sup> series, and K<sup>-40</sup> (Dhanya et al., 2015; Usikalu et al., 2015; Mehra and Bala, 2014).

It is not only feasible but also more essential to assess the radiation hazard by computing indoor external dose by means of experimental and theoretical measurements. As the state-organization of King Abdulaziz City for Science and Technology (KACST) is responsible for radiation protection by performing studies on natural radioactivity in dwellings, this work was mainly devoted and carried out to assess the contents of natural radioactivity in commercial building materials utilized in construction projects in Saudi Arabia. Also, the second aim of the work was to compare the obtained experimental data with Monte Carlo N-Particle (MCNP) mathematical model data.

Doses rates within buildings can only be detected with radiation measuring instruments like the high-resolution gamma-ray spectrometry system which consists of coaxial hyper-pure germanium (HPGe) or NaI detectors. It is also possible to quantify indoor exposure even before the building construction can take place. In this case, mathematical computations for example, MCNP, can be used to evaluate radiation doses from the reported data (Mehra and Bala, 2014; Abdo, 2010).

MCNP is the most widely-utilized method of trusted modeling of external radiation exposure in complex environments such as building materials. MCNP simulation can permit the regarding radiation transport with a very high value of precision. However, the main drawback of MCNP method is the requirement of having high performance computers (Al-Jundi et al., 2009). Koblinger (1978) was the first scientist who used MCNP method within a model to estimate dose rates in air at a point within model room. Although due to low performance of the 70's computers, the model is considered as standard and most highly appreciated model (Romano and Forget, 2013). Other researchers used different approaches. They used various methods of point-kernel integration over volume with analytical methods. The analytical methods can be easily applied for simple geometries whereas MCNP can be used for complex geometries (Zio, 2013).

## EXPERIMENTAL WORK FOR GAMMA ANALYSIS

The collected samples were crushed and then homogenized. The homogenized samples were filled into 1000-ml Marinelli beakers which were later hermetically sealed with the help of commercial polyvinylchloride (PVC) to prevent the escape of airborne Rn-222 and Rn-220 from the samples. All the samples were accurately weighed and stored for a period of at least one month prior to determination in order to attain radioactive secular equilibrium between Ra-226 and Rn-222.

In this study, sample activities in building materials were measured using HPGe detector with highly passive shielding and low background located at KACST. The detector was cooled with liquid nitrogen cryostat to reduce the leakage current. To reduce the background radiation from natural sources, the detector was enclosed in a 10 cm thick cylindrical lead shield. The lead shield was graded with an inner layer of thick copper to reduce any influence of fluorescence. The detector was connected to a pre-amplifier, shaping amplifier and high voltage power supply which were used for conversion of the observed energy into a pulse height spectrum. The pulse amplitude was converted to a discrete number through more 8,000 channel multi-channel analyzer (MCA). The data acquisition, display, and analysis of spectra were carried out using Genie 2000 software.

The relationship between the channel numbers corresponding to absolute energies was determined. The specification of the used instrument is listed in Table 1. In this work, mixed gamma standard containing radionuclides were used for energy set of calibration. Gamma-ray energies covered the range from 50 to 1836 keV. The main gamma-ray energy lines of interest are shown in Table 2. The gamma energies used for Ra-226 was 186.2 keV and different energies of 295.2 and 351.9 keV were also used for Pb-214.

For gamma-ray spectrometry of unknown value, the detector efficiency measurement plays important role in gamma-counting. The full-energy peak efficiency can be computed through:

$$\epsilon_f = \frac{N_p}{N_\gamma} \quad (1)$$

where  $\epsilon_f$  is defined as the full-energy peak efficiency,  $N_p$  is the net gamma-ray counting rate in the full-energy peak,  $N_\gamma$  is defined as the gamma-ray emission rate and can be calculated via:

$$N_\gamma = AP_\gamma \quad (2)$$

where A is the activity in Bq of the reference and P is the branching ratio of the radionuclide.

In order to remove interference between multi peaks, the calibration of energy efficiency was carefully carried. For every source, the energy efficiency was calculated using formula (1) and

**Table 2.** Gamma energies.

Source of gamma ray transition	Gamma emission probability	Gamma-ray energy (KeV)	Identified radionuclide
U-238 series-doublet peak	0.0558 0.0030	92.58	Th-234
Th-232 series	0.0242 0.0009	129.06	Ac-228
Th-232 series	0.0072 0.0002	153.97	Ac-228
Primordial U-235	0.572 0.0005	185.72	U-235
U-238 series	0.0359 0.0019	186.21	Ra-226
Th-232 series	0.0389 0.0007	209.25	Ac-228
Th-232 series	0.4360 0.0030	238.63	Pb-212
Th-238 series	0.0725 0.0002	241.99	Pb-214
Th-232 series	0.0346 0.0006	270.24	Ac-228
Th-232 series	0.0227 0.0003	277.35	Tl-208
Th-238 series	0.1842 0.0004	295.22	Pb-214
Th-232 series	0.0318 0.0013	300.08	Pb-214
Th-232 series	0.0295 0.0012	328	Ac-228
Th-232 series	0.1127 0.0019	338.32	Ac-229
Th-238 series	0.3560 0.0007	351.93	Pb-214
Th-232 series	0.0440 0.0007	463	Ac-228
Annihilation radiation		511	Annihilation
Th-232 series	0.3055 0.0017	583.19	Tl-208
U-238 series	0.4549 0.0016	609.31	Bi-214
Man-made	0.8510 0.0020	661.65	Cs-137
Th-232 series	0.0674 0.0012	727.33	Bi-212
U-238 series	0.0489 0.0001	768.35	Bi-214
Th-232 series	0.0425 0.0007	794.94	Ac-228
Th-232 series	0.0448 0.0004	860.56	Tl-208
Th-232 series	0.2580 0.0040	911.2	Ac-228
U-238 series	0.0311 0.0001	934.06	Bi-214
Th-232 series	0.0499 0.0002	964.76	Ac-228
Th-232 series	0.1580 0.0030	968.97	Ac-228
U-238 series	0.1492 0.0003	1120.28	Bi-214
U-238 series	0.0583 0.0015	1238.11	Bi-214
U-238 series	0.0399 0.0001	1377.67	Bi-214
U-238 series	0.0239 0.001	1407.98	Bi-214
Primordial K-40	0.1066 0.0013	1460.83	K-40
Th-232 series	0.0322 0.0008	1588.19	Ac-228
Th-232 series	0.0151 0.0003	1620.5	Bi-212
U-238 series	0.0298 0.0001	1729.59	Bi-214
U-238 series	0.1530 0.0003	1764.49	Bi-214
U-238 series	0.0492 0.0002	2204.21	Bi-214
Th-232 series	0.3585 0.0007	2614.5	Tl-208

the energy channels was calculated.

### MCNP calculations

The used standard living room, room with dimensions of 4 m × 4 m × 3 m (W × L × H), was defined for the proposed model as illustrated in Figure 1. In the room, the floor was covered with ceramic. Thermo-luminescent dosimeter (TLD) position was in the center of the room, precisely 2 m from each wall and 150 cm above the floor. The density of the used building materials was assumed to be 2325 kg per m<sup>3</sup>. The thicknesses of the used building

materials were assumed to be 0.20 m. The calculation of the dose rate conversion factors from our work was carried out based on MCNP code. The free-in air absorbed dose (nGy h<sup>-1</sup>) value in the center of the room was obtained using MCNP in present study as:

$$D = 0.081A_{K-40} + 0.93A_{U-238} + 1.11A_{Th-232} \quad (3)$$

Where: D is the absorbed dose rate in the center of the room, 0.081, 0.93, and 1.1 nGy.kg.Bq are the dose conversion coefficients for K-40, U-238, and Th-232. The  $A_{K-40}$ ,  $A_{U-238}$ , and  $A_{Th-232}$  are the activity levels in unit of Bq/kg of K-40, U-238, and Th-232, respectively.



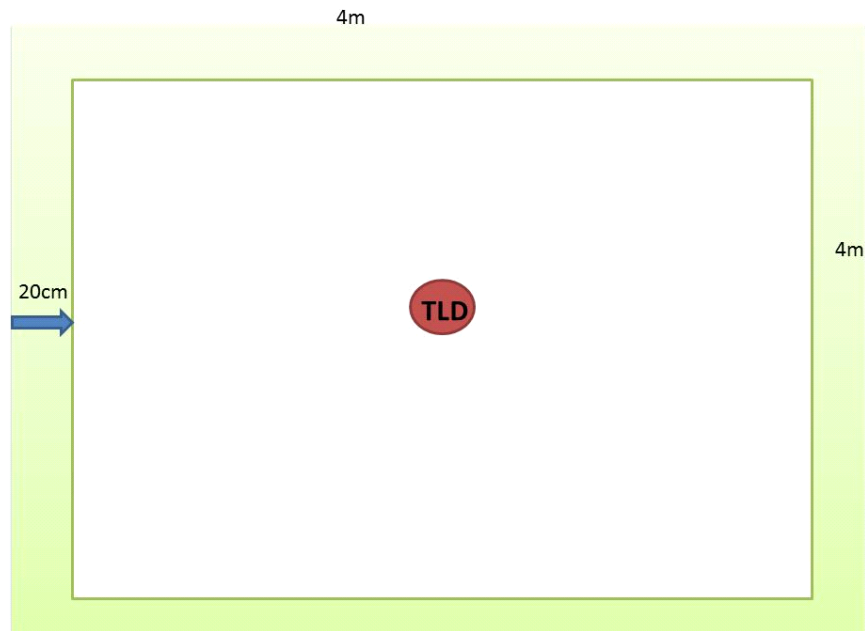


Figure 1. Room geometry model.

To compute the effective dose rate  $E$  in unit of mSv, the conversion factor 0.7 Sv/Gy is required for adult categories. The indoor occupancy factor used by UNSCEAR is 0.8 and the permissible indoor dose is 1 mSv/year. Therefore, the effective annual dose rate can be calculated via (Boda et al., 2013; Ravisankar et al., 2012; Atwood, 2013):

$$E(nSv) = D * 0.7(Sv/Gy) * 0.8 * 24 * 365(h/yr) \quad (4)$$

## RESULTS AND DISCUSSION

Equation 3 obtained in the present work was compared with the ones reported in literature using MCNP method. Table 3 shows the dose evaluation was computed by direct measurement and from MCNP values reported by different authors. K-40 absorbed dose rate was experimentally 0.081 (nGy/h/Bq/kg) whereas the average reported values in literature was 0.079 (nGy/h/Bq/kg). Therefore, statistically the difference between the research's K-40 value and literature value was less than 2%. Similarly, U-238 absorbed dose rate was computed in this work to be 93 (nGy/h/Bq/kg) and the literature value was on the average 0.75 (nGy/h/Bq/kg). Moreover, Th-232 absorbed dose rate was 1.11 (nGy/h/Bq/kg) and the literature value reported in Table 3 was 1.09 (nGy/h/Bq/kg). Thus, the error in case of Th-232 absorbed dose rate between our reported results and literature values was less than 2%. It can be concluded that the present obtained results in Equation 3 are comparable to the values reported by different authors in Table 3. The induction of the present model and other well-known reported models in the literature implies that

the present model and assumptions are in best agreement with other models.

In order to visualize the obtained simulated and experimental results, Figure 2 clearly indicated no difference between the simulated and experimental models owing to the fact that the regression line in Figure 2 is almost very close to a unit and implies that there is an excellent positive correlation between this experimental results and the simulated values. Therefore, MCNP simulation was found to be able to quantify the gamma ray and the absorbed dose in air for any marble materials. The gamma radiation due to natural radioactivity should be evaluated for room dimensions. The simulation results are in good agreement with experimental results.

For ceramic materials, the maximum annual effective dose was approximately 1.7 mSv/year which is slightly elevated while the min value was 0.9 mSv/year, as reported in Table 4. The ceramic materials were still in acceptable range of mode value of safe side although the max value was over a unit. As always expected, adhesive materials are made out of organic materials where no natural sedimentary materials are added. The annual effective dose value of max value was less than 0.23 mSv/year, which was less than the recommended values (1 mSv/year) by our national regulation and International Commission on Radiological Protection (ICRP).

The studied porcelain materials showed the maximum annual effective dose value of less than 1.41 mSv/year which is slightly above the recommended value of 1 mSv/year by ICRP, whereas the mode annual effective dose value was 0.62 mSv/year. Therefore, in considering

**Table 3.** Comparison of specific absorbed dose rates in publications and present work.

Absorbed dose rate in air (nGy/h.Bq/ kg)			Density (g/cm <sup>3</sup> )	Wall thickness (cm)	Room dimension (mm <sup>3</sup> )	Method used	Reference
Th-232	U-238	K-40					
1.11	0.93	0.081	2.32	20	4x4x3	MCNP	This Research
1.03	0.93	0.078	2.32	20	4x4x2.8	MCNP	Koblinger (1978)
1.11	0.92	0.078	2.35	20	4x4x2.8	Analytical	Stranden (1979)
1.05	0.89	0.078	2.35	20	4x4x2.8	Analytical	Mustonen (1984)
1.21	0.95	0.081	2.35	20	4x4x2.8	Analytical	Ahmad and Hussein (1998)
1.19	0.88	0.08	2.35	20	4x4x2.8	Analytical	Ademola and Farai (2005)
0.92	0.7	0.072	2.35	20	4x4x2.8	Analytical	Máduar and Hiromoto (2004)

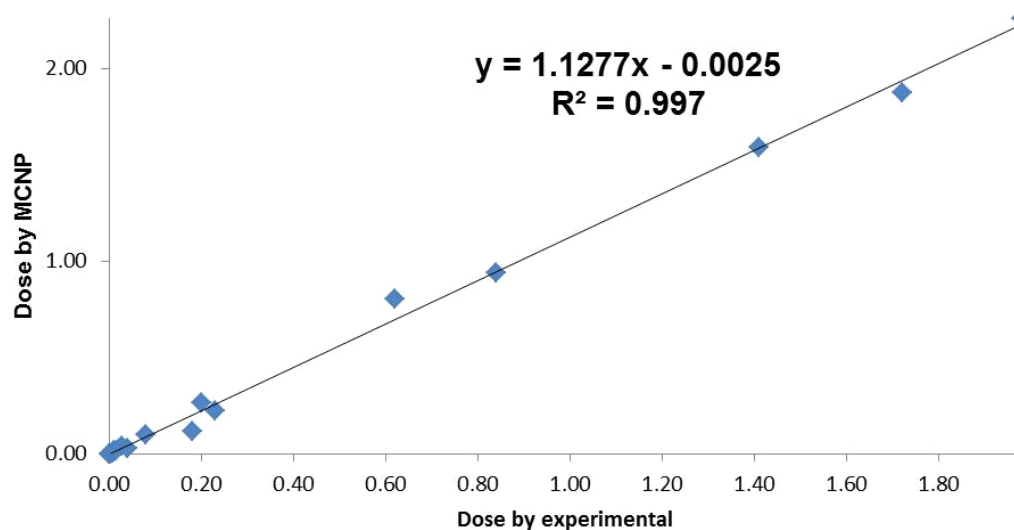


**Figure 2.** Experimental and simulation of gamma radiation effective annual dose

the average value of annual effective dose, one can say that the porcelain materials are free of natural radioactive contaminations.

Similarly, the mode value of annual effective dose of marble materials was approximately 0.2 mSv/year which is slightly below the recommended

value of 1 mSv/year by ICRP. Nevertheless, the max value of annual effective dose was about 2 mSv/year a result that is believed to be high. For paint materials, with similar procedures for adhesive materials, the max value of annual effective dose was less than 0.03 mSv/year and

this value is far below the value of 1 mSv/year by ICRP. Thus, the paint materials are assumed to be safe against radiation hazard. For gypsum materials, the maximum reported value in this work was less than 1.1 mSv/year; hence they are regarded as safe materials for construction.

**Table 4.** Comparison of annual dose of experimental calculations and MCNP calculations.

Material	U-238 (Bq/kg)	SD	Th-232 (Bq/kg)	SD	Ra-226 (Bq/kg)	SD	K-40 (Bq/kg)	SD	Dose by MCNP (mSv/year)	Dose by experimental (mSv/year)
<b>Ceramic</b>										
Mean	65.15		71.3		81		636		0.939	0.84 0.28
Min	0	58	0	46.7	31.12	45	296	285	0.118	0.18
Max	148		136		150		1144		1.872	1.72
<b>Adhesive</b>										
Mean	8.69		7.1		10.49		44.3		0.096	0.08 0.02
Min	0	4.83	4.9	2.2	6.5	3	0	7.9	0.027	0.04
Max	17.4		12.4		18.1		183		0.22	0.23
<b>Porcelain</b>										
Mean	53		61		60		585		0.804	0.62 0.28
Min	0	31	0	32	0	33	43	252	0.017	0.01
Max	116		126		135		939		1.591	1.41
<b>Marble</b>										
Mean	12.1		21.77		13.5		220		0.261	0.2 0.3
Min	0	3.7	0	47.95	0.3	15.85	0	423	0	0
Max	53.8		254		57.7		1588		2.261	1.98
<b>Paint</b>										
Mean	2.27		0.1		2.75		3.2		0.012	0.01 0.01
Min	0	3.93	0	0.17	0.5	3.73	0	0.95	0	0
Max	6.8		0.3		7.05		8.9		0.036	0.029
<b>Gypsum</b>										
Mean	2.7		0.1		2.7		3.2		0.014	0.015
Min	-	10	0	0.01	0.7	4.5	0.7	-	0	0.004
Max	-		0.3		7.05		8		0.005	0.008

## Conclusion

The estimated average annual effective doses were 0.8 mSv/year for ceramics, 0.08 mSv/year

for adhesives, 0.6 mSv/year for porcelains, 0.2 mSv/year for marbles, 0.01 mSv/year for paints, and 0.015 mSv/year for gypsum materials. Fortunately, all of the reported annual effective

dose values of the studied building materials were located within the safe limits of acceptable recommendation of less than 1 mSv/year in accordance with the national regulation and ICRP.


For the second part of this work, the radiation data reported by MCNP code and gamma laboratory showed that the radiation experimental data and radiation simulated data were comparable and matched because the drawn regression between both experimental and simulated data was 99.7%; implying that the matrix correlation between experimental and simulated data are excellently positive.

## CONFLICT OF INTERESTS

The authors have not declared any conflict of interests.

## REFERENCES

- Abdo SYM (2010). The activity concentrations for some building materials in Yemen and simulation of the indoor gamma dose rate. The Degree of Master of Science Nuclear physics, Physics Department, Faculty of Science, Cairo University.
- Ademola J, Farai I (2005). Annual effective dose due to natural radionuclides in building blocks in eight cities of southwestern Nigeria. *Radiat. Prot. dosimetry* 114(4):524-526.
- Al-Jundi J, Ulanovsky A, Pröhl G (2009). Doses of external exposure in Jordan house due to gamma-emitting natural radionuclides in building materials. *J. Environ. Radioact.* 100(10):841-846.
- Ahmad N, Hussein A (1998). Radiation doses in Jordanian dwellings due to natural radioactivity in construction materials and soil. *J. Environ. Radioact.* 41(2):127-136.
- Atwood DA (2013). *Radionuclides in the Environment*, John Wiley & Sons.
- Boda D, Csányi É, Gillespie D, Kristóf T (2013). Dynamic Monte Carlo simulation of coupled transport through a narrow multiply-occupied pore. *J. Phys. Chem. C* 118(1):700-707.
- Dhanya B, Umadevi AG, Jose PA, JoJo PJ, Harikumar M, Sujata R (2015). Assessment of natural radioactivity level and radiation hazard parameters in the terrestrial environment of Eloor Island, Kerala. *Int. J. Fund. Phys. Sci.* 5(2):38-42.
- Koblinger L (1978). Calculation of exposure rates from gamma sources in walls of dwelling rooms. *Health Phys.* 34(5):459-463.
- Máduar MF, Hiromoto G (2004). Evaluation of indoor gamma radiation dose in dwellings. *Radiat. Prot. Dosimetry* 111(2):221-228.
- Mehra R, Bala P (2014). Assessment of radiation hazards due to the concentration of natural radionuclides in the environment. *Environ. Earth Sci.* 71(2):901-909.
- Mustonen R (1984). Methods for evaluation of radiation from building materials. *Radiat. Prot. Dosimetry* 7(1-4):235-238.
- Ravisankar R, Vanasundari K, Chandrasekaran A, Rajalakshmi A, Suganya M, Vijayagopal P, Meenakshisundaram V (2012). Measurement of natural radioactivity in building materials of Namakkal, Tamil Nadu, India using gamma-ray spectrometry. *Appl. Radiat. Isot.* 70(4):699-704.
- Romano PK, Forget B (2013). The OpenMC Monte Carlo particle transport code. *Ann. Nucl. Energy* 51:274-281.
- Stranden E (1979). Radioactivity of building materials and the gamma radiation in dwellings. *Phys. Med. Biol.* 24(5):921.
- Usikalu MR, Maleka PP, Malik M, Oyeyemi, KD (2015). Assessment of geogenic natural radionuclides contents of soil samples collected from Ogun State, Southwestern Nigeria. *Int. J. Rad. Res.* 13(4):355-361.
- Zio E (2013). *The Monte Carlo simulation method for system reliability and risk analysis*, Springer. DOI: 10.1007/978-1-4471-4588-2.



# International Journal of Physical Sciences

## Related Journals Published by Academic Journals

- *African Journal of Pure and Applied Chemistry*
- *Journal of Internet and Information Systems*
- *Journal of Geology and Mining Research*
- *Journal of Oceanography and Marine Science*
- *Journal of Environmental Chemistry and Ecotoxicology*
- *Journal of Petroleum Technology and Alternative Fuels*

**academicJournals**